

Volume Uptake of Carbonyls during Diffusional Ice Crystal Growth

Jackson Seymore^{*1}, Miklós Szakáll¹, Alexander Theis³, Subir K. Mitra³, Christine Borchers², Thorsten Hoffmann²

¹ Institute for Atmospheric Physics, Johannes Gutenberg University, Mainz, Germany

² Department of Chemistry, Johannes Gutenberg–University, Mainz, Germany

³ Particle Chemistry Department, Max Planck Institute for Chemistry, Mainz, Germany

*Corresponding author: Jackson Seymore seymorej@uni-mainz.de

Keywords: volume uptake, gas-ice partitioning, diffusional crystal growth, Orbitrap MS, secondary organic aerosol, SOA, convective clouds, entropy-enthalpy compensation, EEC

Abstract

Carbonyls are highly relevant atmospheric constituents that influence tropospheric photochemistry and oxidative capacity. They can be removed from the upper troposphere via ice phase deposition scavenging. The gas-volume uptake coefficients for 14 different carbonyl compounds were determined using a flowtube apparatus. Ice crystals were grown from vapor deposition in the presence of gas phase carbonyls at -20 , -30 , and -40 °C. Using van't Hoff analysis, the entropy and enthalpy of uptake were determined. An inverse relationship between uptake coefficients and temperature was observed for all species except methyl vinyl ketone. A linear correlation between ΔS and ΔH arose which was statistically validated and determined with 99% confidence to not be a statistical artifact. This compensation behavior could be an indication of a surface liquid layer or quasi-liquid layer behavior involved in the uptake process and could also indicate a single dominant influence on a compound's uptake. The most significant physicochemical properties correlated with uptake were identified to be vapor pressure and molar mass, which indicate that smaller compounds with higher vapor pressures are more readily taken into the ice phase. The volume uptake coefficients observed here are below the $10 \text{ mol m}^{-3} \text{ Pa}^{-1}$ threshold given by Crutzen and Lawrence (2000) to be considered a substantial atmospheric removal process.

1 Introduction

Scavenging of organic gases by hydrometeors—such as rain, snow, graupel, and cloud droplets—has a cleaning effect on the atmosphere. While Henry's law coefficients are available to describe the interactions with

30 most organic gases with liquid water (Sander, 2023), less is known about its interactions with ice phase deposition. Most precipitation in the midlatitudes as well as all cloud formation in the upper troposphere is formed via ice and subsequently indicates that ice is a significant contributor to the wet deposition of trace atmospheric constituents (Franz and Eisenreich, 2000; Heymsfield et al., 2020; Mülmenstädt et al., 2015). Ice growth in the atmosphere operates under a few distinct processes: (1) the collection of supercooled cloud droplets by ice (riming), (2) direct
35 liquid freezing, and (3) vapor-to-ice growth by diffusion. The latter process—often referred to as depositional growth—is hereafter referred to as diffusional growth and is the responsible mechanism for all cloud formations in the upper troposphere (Heymsfield et al., 2020; Mülmenstädt et al., 2015). There has been significant research in recent years on the redistribution and revolatization of organics during riming or liquid freezing (Borchers et al., 2024; Jost et al., 2017; Gautam et al., 2025; Seymore et al., 2025), but very little for diffusional growth.

40 Carbonyls as a class of trace atmospheric constituents are highly relevant secondary organic aerosol (SOA) precursors and intermediates (Ervens and Kreidenweis, 2007; Galeazzo et al., 2024; Srivastava et al., 2022; Yu et al., 2014). They are ubiquitous and play vital roles in tropospheric photochemistry and oxidative capacity, which affects radical cycling and ozone formation (Xu et al., 2023). Specifically, the photolysis of carbonyls is an important source of peroxy radicals in the atmosphere. After photolysis, the aldehydic group (-CHO) decomposes and forms
45 the HO₂ radical with the addition of O₂. This peroxy radical is then a source of atomic oxygen for ozone formation (Liu et al., 2022). Formaldehyde, acetaldehyde, and acetone are typically the most abundant and considered the main contributors to ·OH reactivity and dominate the ozone formation potential of the total oxygenated volatile organic compounds (VOC), while less abundant species like benzaldehyde make a minor contribution to the ·OH removal rate and inhibit ozone formation (Wang et al., 2022). Additionally, lower vapor pressure carbonyls can be oxidized
50 to form SOA through gas-particle partitioning. This chemical evolution and physical transformation results in a range of lifetimes for various carbonyls from hours (e.g., below 1 hr for unsaturated aldehydes against OH oxidation, 1–3 hr lifetime for glyoxal against photolysis and OH oxidation, 1.3 hr for formaldehyde and glyoxal under overhead sun conditions) to a few days (i.e., 15 days for acetone with respect to the oxidation by OH) depending on their structures (Jacob, 2021). Compounds like glyoxal and methylglyoxal are significant contributors
55 to SOA formation via aqueous-phase chemistry (Ling et al., 2020) and many other such SOA contributing carbonyls are isoprene products, like methacrolein, methyl vinyl ketone (MVK), hydroxyacetaldehyde, or hydroxyacetone (Grosjean et al., 1993). Nopinone, diacetyl, camphor, norcamphor, and propionaldehyde are other naturally

occurring carbonyls of interest that present a variety of structures and properties for comparison. Notably nopinone, camphor, norcamphor, and propionaldehyde are analogous bicyclic monoterpenoids while diacetyl is another
60 diketone similar to glyoxal and methylglyoxal.

Despite their relevance, there are limited studies describing their removal from the upper atmosphere via deposition scavenging and only then describe their resultant wet deposition (Bartels-Rausch et al., 2014; Mu and Xu, 2009). Huffman and Snider (2004) attempted to measure uptake of acetone as a representative for ketones as hydrogen bond acceptors, however background contamination prevented thorough characterization. They did,
65 however, publish a volume uptake coefficient for acetone and concluded that it had a significantly lower uptake than the alkanols studied.

The publications by Fries et al. (2007) and Huffman and Snider (2004) concern the ice uptake of aromatic hydrocarbons and oxyhydrocarbons. These are the first studies to describe the interactions between diffusion-growing ice and depositing organic vapors. Outside of these, the only measurements for diffusional uptake are for
70 select inorganic species (e.g. H₂O₂, HCl, HNO₃, etc.) (Bartels-Rausch et al., 2014; Conklin et al., 1993; Diehl et al., 1995; Dominé and Thibert, 1996; Mitra et al., 1990; Santachiara et al., 1998) or adsorption on nongrowing ice (Abbatt et al., 2008; Von Hessberg et al., 2008). These experiments to evaluate gas interactions with ice describe either “growing ice” or “static ice” which have investigated the effects of volume uptake and surface processes respectively. From this distinction, these publications reveal that many uptake processes are predominately volume
75 uptake with secondary contributions from certain surface processes, notably (1) bonding to the air-ice interface or (2) uptake into a liquid solution phase coexisting with ice (Conklin et al., 1993; Goss, 1993). Further, they show that equilibrium treatments of both surface and volume uptake can correctly predict the resulting concentrations in snow (Dominé and Thibert, 1996).

Treating the uptake of organic compounds by ice crystals growing through diffusion as an equilibrium
80 allows for the calculation of gas-ice partitioning coefficients, referred hereafter as uptake coefficients. These coefficients ($K_{g,ss}$) describe the ratio of the gas phase concentration of the analyte vapor to its concentration in the ice phase. More specifically, with the possibility for a liquid solution phase that coexists with ice, this relationship is described as:

$$K_{g,ss} = K_{g,l}K_{l,ss} \quad (1)$$

where the equilibrium constants $K_{l,ss}$ and $K_{g,l}$ relate the analyte concentrations in the ice solid solution (ss) and liquid water (l) phases to the analyte partial pressure in the gas phase (g). The last equilibrium constant ($K_{l,ss}$) relates the concentrations in the liquid water (l) and solid solution (ss) phases. The present study reports direct measurements of $K_{g,ss}$ for carbonyl compounds and neglects thorough investigation of gas to liquid or liquid to ice equilibrium. Hereafter, $K_{g,ss}$ will be referred to simply as K and is specifically considered a volume uptake coefficient.

In the present study, laboratory experiments explore the uptake of 14 different carbonyl species by ice crystals during vapor deposition growth. Ice crystals were grown from vapor deposition under controlled humidity conditions in the presence of gaseous carbonyl species. The blended gas mixture was targeted to produce roughly 10 ppbv of each gaseous analyte to maintain analytical reliability, approximately ~~21–32~~ orders of magnitude larger than the partial pressures of these compounds in the unpolluted troposphere. Water vapor saturation was controlled to 50% supersaturation (wrt ice) to achieve realistic growth conditions in natural cirrus clouds. Gas phase concentrations were determined using an integrative denuder technique and subsequent derivatization to aid detection for both gas and ice phase concentrations. Ultra-high performance liquid chromatography with ultra-high resolution mass spectrometry (UHPLC-UHRMS) was then used to analyze the samples and determine their uptake coefficients.

2 Methods

2.1 Experimental Setup

The experimental design in this paper is a variation on the experiment presented by Fries et al. (2007) with gas measurement techniques developed by Kahnt et al. (2011). In the present experiment, ice crystals are grown in the presence of carbonyl vapors. Their concentrations in the ice-phase and the gas phase are then measured to determine their uptake coefficients.

Three uptake experiments were performed with three replicates at atmospheric pressure with the experimental apparatus shown in Figure 1. The setup had three main stages: an ambient temperature gas-mixing stage, a chilled crystal growth flowtube, and outflowing gas measurement. In the first stage (Stage 1. Gas Mixing), pressurized dry nitrogen gas was passed through a bubbler with known concentrations of the analytes in aqueous

solution. This stream of gas then reached saturation at ambient temperature (maintained at 23 °C and confirmed by measurement) and passed through a glass frit and a droplet catching chamber to ensure no liquid droplets remained in the gas stream. The saturated gas stream was then diluted with dry nitrogen to reach the desired humidity and vapor concentration. The specific saturation and vapor concentration mix was maintained using a Mass Flow Controller (Brooks Instrument B.V. 5850TR/FA1B201). The resulting mixed gas was allowed to homogenize inside a 0.5 L mixing chamber and then was introduced into the insulated chamber with the crystal growth tube. Another Mass Flow Controller was used to ensure a constant volumetric flowrate was maintained through the flowtube and through a branching line for input gas measurement.

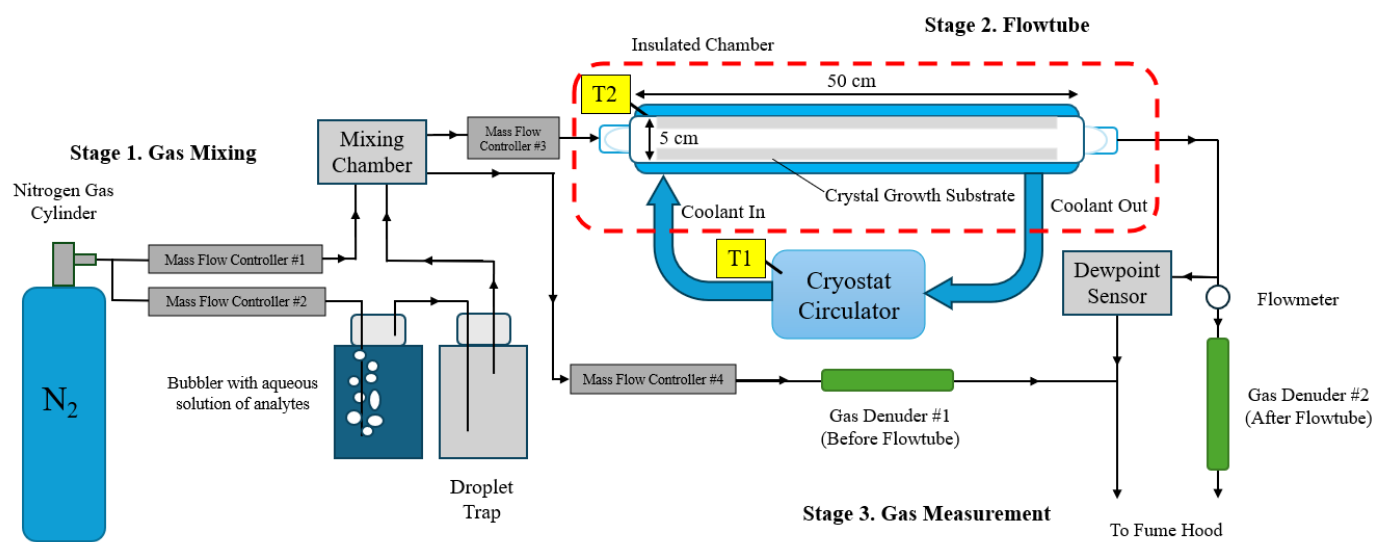


Figure 1. Experimental Apparatus Design

The second stage of the apparatus is the flowtube portion of the setup (Stage 2. Flowtube). The flowtube is a quartz-glass tube of 50 cm length and 5 cm diameter with an approximate interior volume of 1 L where ice crystals were grown from diffusional vapor deposition. It is capped at both ends with a uniform flow PTFE nozzle with double silicon VMQ O-rings to ensure proper sealing of the gas stream at low temperatures. The flowtube is inserted into a copper thermal exchange coil with a PT100 temperature sensor (T2) mounted between the coil and the tube. The flowtube and coil are housed inside an insulated chamber while ethanol coolant is circulated through the coil from a cryostat circulator (Julabo F81) outside the chamber. Using the coolant bath temperature (T1) and T2, the

temperature of the flowtube glass substrate can be maintained within 0.1 C of the target temperature using PID control. Prior to each experiment, the flowtube substrate is ethanol cleaned, dried with nitrogen gas, and brought to the target temperature under the flow of dry nitrogen. This prevents ice nucleating contaminants and ambient humidity from depositing on the substrate prior to exposure to the test gas. The flowtube is allowed to cool for 1 hour prior to exposure to ensure temperature stability. This setup was also thermally characterized using a PT100 sensor mounted on a probe inserted along the center of the tube. The quantitated temperature error was determined using this method and the resulting temperature profiles can be found in Figure S1 of the Supplemental Materials.

After the flowtube is the third stage of the setup where the effluent gas is analyzed (Stage 3. Gas Measurement). Continuous dewpoint measurements along with an integrative measurement of vapor analytes were taken on the before and after flowtube gas streams using a dewpoint hydrometer (Michell Instruments S8000) and a pair of reagent-coated gas denuders. Ice samples were collected from the flowtube, weighed, and analyzed for their analyte concentration. This data is then able to be used to calculate the uptake coefficient. PTFE tubing was used for all the tubing connections and the flow conditions in these experiments remained laminar with a Reynolds number of approximately 160, which is well below the critical value of 2300 for pipe flow (Warhaft, 1998). Experiments were performed 24 hours at -20 and -30 °C, 48 hours for -40 °C to allow for adequate crystal growth and saturation of any vapor wall losses.

2.2 Crystal Growth Conditions

Ice crystals were grown from vapor deposition under controlled humidity conditions in the presence of gaseous carbonyl species. For the experimental temperatures of -20 , -30 , and -40 °C, ice was grown at 50% supersaturation (wrt ice) with 10 ppbv of analyte vapor (140 ppbv total organics). To achieve these target conditions, different dilutions of dry nitrogen with the saturated gas stream were mixed using different bubbler solutions with the required aqueous concentrations of analytes to reach the target partial pressure. The saturation pressure of water vapor over ice (e_i) was calculated using the Sonntag parameterization (Sonntag, 1994) so that the saturation ratio of water vapor with respect to ice (S_{ice}) was maintained at 1.50 at experimental temperatures of -20 , -30 , -40 °C. This S_{ice} was chosen as it is a high but realistic saturation for the growth conditions in natural cirrus clouds (Comstock et

al., 2004; Dekoutsidis et al., 2023; Hoareau et al., 2016; Zhao and Shi, 2023) with a similarly realistic temperature range that still allows for high enough water vapor pressures and crystal growth rates to be experimentally viable.

For the gas stream mixing, this was first theoretically calculated as a dilution of saturated bubbler water vapor (19.42 g m⁻³ at 23 °C) with dry gas (< 0.03 g m⁻³) to within 10% error. This was also then empirically determined by measuring the mixed gas dewpoint, calculating the water vapor pressure using the Sonntag parameterization and adjusting the flowrates accordingly.

The crystal growth rate (J) was calculated using a Fick diffusion term:

$$J = D_T \frac{C_0 - C_f}{l_m} \quad (2)$$

where l_m is the thickness of the diffusion layer, D_T is the diffusion coefficient of water vapor (2.2×10^{-5} m² s⁻¹) and C_0 and C_f are the input and output water vapor concentrations. The value of l_m is calculated by the Einstein equation:

$$l_m = \sqrt{2D_T t_k} \quad (3)$$

where t_k is the condensation time, i.e. residence time within the flowtube. l_m was estimated to be 0.025 m, which is roughly the interior radius of the flowtube. J is then multiplied by the interior surface area of the flowtube substrate (approximately 785 cm²) to produce the total ice growth rate in the flowtube. While the crystal growth rate was theoretically calculated for all experiments, it was also empirically determined by dividing the sampled ice mass by the total experiment time.

With the experimental humidity determined and the flowrates fixed, the gas dilution factor of the bubbler gas is then also fixed. From this, the aqueous concentrations of all the analytes in the bubbler that produce the desired vapor concentrations in the flowtube can be determined. Using Henry's law and the compiled Henry's law constants and calculations from Sander (2023), (provided in Table S1 in the Supplemental Materials), the necessary aqueous concentrations to produce 10 ppbv of analyte vapor in the flowtube were determined. 10 ppbv was selected as the analyte vapor mixing ratio as it was a low mixing ratio that could still maintain signal in the ice samples. The Henry's law constant was first adjusted to ambient conditions using the equation:

$$H_T = H^\theta \cdot \exp\left(\frac{-\Delta_{sol}H}{R}\left(\frac{1}{T} - \frac{1}{T^\theta}\right)\right) \quad (4)$$

Here, Henry solubility (H^θ) at the reference temperature (T^θ) and the molar enthalpy of dissolution ($\Delta_{sol}H$) are used along with the gas constant (R) and ambient temperature (T) to correct to the Henry solubility (H_T). With the concentration/pressure defined H_T adjusted to ambient conditions, the aqueous concentration of the analyte in the bubbler necessary to produce the desired amount of gas-phase analyte in the flowtube can be calculated using the equation:

$$[x]_{aq} = H_T^{cp} \cdot p_x^{FT} \cdot d \quad (5)$$

where the dilution factor (d) corrects the partial pressure of x analyte in the flowtube (p_x^{FT}) to the partial pressure required in the bubbler due to the gas mixing dilution to provide the aqueous concentration ($[x]_{aq}$). These concentrations are stable in the bubbler, assuming that the mass fraction in the aqueous phase is much larger than the mass fraction in the vapor phase. The actual aqueous concentrations and Henry solubilities used can be found in Table S1 the Supplementary Materials. While these calculations were performed to reach a target partial pressure of 10 ppbv, the actual partial pressure in the flowtube was determined by dividing the mass of analyte collected on the reagent-coated gas denuders and dividing by the total volume passed through the denuders. Corrections for mass error due to the breakthrough potential of a species through the denuder were made following the same method as (Kahnt et al., 2011). The average breakthrough potential for all species under these conditions was determined to be less than 4%. While Kahnt et al. (2011) observed much higher breakthrough potentials than this at lower relative humidities than in these experiments, the absolute humidity in these experiments is lower by 5 orders of magnitude. Since water can both encourage and inhibit the derivatization, any changes in humidity conditions may alter the breakthrough potential of any of the analytes.

2.3 Chemicals and Materials

The derivatization reagent 2,4-dinitrophenylhydrazine (DNPH) was purchased from Sigma-Aldrich (~0.2 M, ~4% Phosphoric acid solution, Darmstadt, Germany). The denuder coating solution was prepared with 10 mM DNPH in acetonitrile (ACN). The following carbonyl compounds were obtained from Sigma-Aldrich (St. Louis, MO, USA): benzaldehyde (≥99%), methacrolein (95%), norcamphor (98%), (1R)-(+)-nopinone (98%), and methyl

205 vinyl ketone (MVK, with 0.5% hydroquinone and 0.1% acetic acid). Formaldehyde (30%, methanol-free) and
acetaldehyde ($\geq 99\%$) were obtained from Roth (Karlsruhe, Germany). Hydroxyacetone (95%) and propionaldehyde
(97%) were obtained from Thermo Scientific (Darmstadt, Germany). Glyoxal (39% in water) and diacetyl ($>98\%$)
were purchased from TCI (Toshima, Tokyo, Japan). Methylglyoxal (40% in water) was purchased from MP
Biomedicals (Irvine, CA, USA). d/l-camphor (97.5%) was obtained from WHI pharma services (Frankfurt,
210 Germany). These compounds were used without further purification. For the aqueous bubbler solution, 98 % LC/MS
grade water (Thermo Fisher Scientific) was used for the solvent and $>99.8\%$ technical grade nitrogen was used for
the carrier gas.

Supelco carbonyl-DNPH mix 13, a commercially available hydrazone standard solution, was purchased
from Sigma-Aldrich and used for the analysis of benzaldehyde, MVK, methacrolein, acetaldehyde, formaldehyde,
215 acetone, and propionaldehyde. Hydrazone crystals were prepared for benzaldehyde, nonpinone, norcamphor,
camphor, diacetyl, glyoxal, hydroxyacetone, and methylglyoxal. Benzaldehyde-DNPH was purified by
recrystallization from ethanol and then prepared in ACN. All other synthesized carbonyl-DNPHs were purified using
a solid phase extraction (SPE) method (Chromabond® C₁₈, 6 mL, 1000 mg bedweight) and then referenced to the
prepared benzaldehyde-DNPH standard with UHPLC-HRMS. This was then referenced to the Supelco standard.
220 The difference in the signal was about 23% ($n = 6$) between commercial and synthesized benzaldehyde-DNPHs
confirming the concentration of the benzaldehyde-DNPH. Since the uptake partitioning coefficients are unitless and
the sample matrices are the same, only relative quantitation is necessary for the calculation. This circumvents the
need for true quantitation as referenced to an external standard. However, since these standards are referenced to the
Supelco standard, true quantitation was performed for benzaldehyde, MVK, methacrolein, acetaldehyde,
225 formaldehyde, acetone, and propionaldehyde and pseudo-quantitation (estimating concentration by referencing
signal intensity to an internal standard) was performed for nonpinone, norcamphor, camphor, diacetyl, glyoxal,
hydroxyacetone, and methylglyoxal.

2.4 Sample Collection and Preparation

230 Three samples were collected from each experiment: input gas denuder extract, output gas denuder extract,
and ice. These samples were treated with a derivatization reagent and concentrated in preparation for analysis. The

gas denuders were prepared in the method described by Kahnt et al., (2011). Two 5-channel annular denuders with 750 mm length and 1 mm annular spacing (URG 4531, URG Corporation, Chapel Hill, NC, USA) were coated with XAD-4 resin following the method presented by Kahnt et al. (2011) and then coated with DNPH before immediate use. The resin coating was renewed after five experiments. At the conclusion of the experiment, the denuder samples were directly extracted three times with 50 mL of ACN by capping and inverting twenty times while rotating along its axis. These samples were then left overnight to ensure complete derivatization.

Ice samples were collected by methanol extraction of the flowtube. At the conclusion of the experiment, the flowtube and thermal exchange coil were sealed, disconnected from the setup, and taken into a walk-in cold chamber kept at -5°C . The caps were removed from the flowtube and the interior was rinsed with 14 mL of anhydrous methanol. The flowtube extract was weighed and then the water content was determined by measuring the refractive index using an Abbe refractometer. Knowing the percent water content (w/w%) of the extract and the total mass of the extract (g), the ice yield could be determined (g). This extract was then spiked with 0.1 mL of the DNPH solution and left overnight to ensure complete derivatization. This method prevents deposition by ambient humidity onto the flowtube substrate and is a more efficient recovery method than physical scraping, which was not a viable method due to the low ice masses deposited.

The samples were then all concentrated by rotary evaporation (25°C at 150 mbar) and were reconstituted in 1 mL of methanol to be purified by SPE (Chromabond® C₁₈, 6 mL, 1000 mg bedweight). The cartridges were first flushed with 6 mL ACN, conditioned with 3 mL methanol and 6 mL of ultra-pure water. The denuder extract was loaded on the SPE cartridge and washed with 3 mL of methanol/water solution (5/95%, v/v%) to remove any phosphoric acid. The carbonyl-DNPHs were eluted using 10 mL ACN and stored out of light at -25°C in a deep freezer. For analysis, 0.25 mL of the output gas denuder extract, 0.5 mL of the input gas denuder extract, and 1 mL of the ice sample were taken and evaporated to dry in a nitrogen evaporator at 18°C . These were reconstituted to 0.5 mL ACN/H₂O (50/50, v/v%) for ultra-high-performance liquid chromatography coupled with high resolution mass spectrometry (UHPLC-HRMS). The dilution/concentration for these respective samples were performed to bring the expected concentration into quantitation range.

2.5 UHPLC-HRMS Analysis

Analysis was performed in triplicate using a Dionex UltiMate 3000 ultra-high-performance liquid chromatography (UHPLC) system coupled to a heated electrospray ionization source (HESI) and a high-resolution Q-Exactive Orbitrap mass spectrometer (HRMS) (all Thermo Fisher Scientific). A Hypersil Gold, C18, 50 x 2.0 mm column with 1.9 μm particle size (Thermo Fisher Scientific) was used for the chromatography. Eluent A consisted of 98 % LC/MS grade water (Thermo Fisher Scientific) with 0.04 % formic acid and ACN (VWR Chemicals), eluent B consisted of 98 % ACN and water, and the injection volume was 10 μL . Column temperature was held at 40 $^{\circ}\text{C}$. The HESI source was used in negative mode, resulting in the formation of deprotonated molecular ions. Sheath gas and auxiliary gas pressure was 40 and 20 a. u. (arbitrary unit) respectively. The temperature of the auxiliary gas heater was 150 $^{\circ}\text{C}$ and the capillary temperature was 350 $^{\circ}\text{C}$. The sprayer voltage was set to -4.00 kV . To further enhance ionization, a post-column flow of 50 mmol L^{-1} NH_4OH in MeOH was added after 1 min at a flow rate of 0.1 mL min^{-1} . The following $\text{H}_2\text{O}/\text{ACN}$ chromatography gradient was used: Starting with 30% B isocratically for 1 min, increasing to 80% at 10 min, then to 100% at 11 min, and back to 30% B at 11.5 min allowed to equilibrate to initial conditions for 1 min. The first minute of eluent was ejected to waste to reduce excess unreacted DNPH being fed into the HRMS. The mass traces used to identify the species in this experiment can be found in Table S2 in the Supplementary Materials.

2.6 Calculations

The partitioning coefficient between the gas and ice phase K was calculated by the equation:

$$K = \frac{\rho_{ice}C_{ice}}{m_{ice}C_{gas}} \quad (6)$$

where C_{ice} is the absolute mass of the analyte in ice (ng), ρ_{ice} is the density of ice at the experimental temperature (0.9194, 0.9200, 0.9208 g cm^{-3}), C_{gas} is the concentration of the analyte in the gas phase (ng m^{-3}), and m_{ice} is the total mass of ice (g). For proper unit conversion, a factor of 10^6 is applied for the conversion of m^3 to cm^3 . Practically speaking, the uptake coefficient K can also be used as a sorption coefficient or a dimensionless uptake coefficient with respect to the removal of trace gases in the upper atmosphere. A larger value for K indicates more uptake into the ice phase.

Strictly speaking, chemical uptake on growing ice crystals is a stationary state and not an equilibrium. However, diffusional crystal growth is slow relative to other modes of freezing (day vs. ms timescales) and so the system can be approximated as an equilibrium state (Dominé and Thibert, 1996; Fries et al., 2007; Huffman and Snider, 2004). Then as a thermodynamic equilibrium, K can also be used to calculate the Gibbs energy (ΔG) of the uptake process at each temperature. This is a direct calculation using the equation:

$$\Delta G = -RT\ln(K) \quad (7)$$

where T is temperature (K) and R is the ideal gas-constant ($8.31447 \text{ J K}^{-1} \text{ mol}^{-1}$). These values describe the thermodynamic potential of the uptake process. Positive values of ΔG indicate the analyte proceeds spontaneously to the gas phase while negative values of ΔG indicate the analyte proceeds spontaneously to the ice phase provided similar magnitudes of ice and gas volumes. Even lower, more negative values of ΔG would indicate more efficient uptake of the analyte into the ice phase provided the available ice volume is sufficient.

Continuing the thermodynamic analysis, the theoretical temperature dependence of the uptake coefficient K —used in place of a sorption coefficient—can be determined with the van't Hoff equation, which when substituting with the Gibbs-Helmholtz equation produces the following:

$$\ln(K) = -\frac{\Delta H - T\Delta S}{RT} = -\frac{\Delta H}{R} \frac{1}{T} + \frac{\Delta S}{R} \quad (8)$$

where ΔH and ΔS are the heat of sorption and the sorption entropy respectively. Here the heat of uptake and uptake entropy are used instead. Performing a linear regression of $\ln(K)$ against $1/T$ using the van't Hoff equation provides a slope of $-\Delta H/R$ and an intercept of $\Delta S/R$. Multiplying each of these values by $-R$ and R respectively produces the values of ΔH and ΔS . Increasing values of the uptake enthalpy ΔH and the uptake entropy ΔS along with decreasing compound vapor pressure—i.e. the volatility of the pure analyte—can indicate that the uptake of the analyte is dependent on the physical parameters of the compounds and ice surface. Specifically, these are the parameters that determine thermodynamic sorption such as temperature, molecular mass, ice surface coverage, surface morphology and porosity, surface crystallographic phases, quasi-liquid layer behavior, and crystal imperfections (Behr et al., 2006; Fries et al., 2006; Orem and Adamson, 1969; Sokolov and Abbatt, 2002). However, lower values of ΔH and poor linear regression can be a sign that the uptake process cannot be exclusively described by thermodynamic sorption.

3 Results and Discussion

3.1 Ice Crystal Growth

Nine ice samples were grown in the presence of vapor phase carbonyl compounds. While the target partial pressure for each species was 10 ppbv, the actual (excluding glyoxal) concentrations as referenced against denuder #1 was 11.5 ± 2.5 ppbv on average. The actual partial pressure for each species can be found in the Supplemental Materials. The typical ice yield at -20 °C was calculated to be roughly 3.07 g while the actual yield was measured to be 5.77 ± 0.45 g on average. The corresponding theoretical and actual crystal growth rates were 128.1 mg hr^{-1} and 237.8 mg hr^{-1} at 1.55 ± 0.14 hPa water vapor pressure (49.9 ± 13.8 % S wrt ice). For -20 °C, the actual ice yield measurement is strictly an overestimate as the refractive index measurement was closest to the parabolic vertex of the water-MeOH mixture where small deviations in the refractive index produce large differences in the estimated water content. At -30 °C, the calculated ice yield was 1.13 g while the average actual yield was 1.07 ± 0.52 g. The corresponding theoretical and actual crystal growth rates were 47.1 mg hr^{-1} and 44.6 mg hr^{-1} at 0.57 ± 0.05 hPa water vapor pressure (49.6 ± 14.1 % S wrt ice). For -40 °C, the calculated ice yield was 0.79 g while the actual was 0.57 ± 0.11 g. The corresponding theoretical and actual crystal growth rates were 16.4 mg hr^{-1} and 11.8 mg hr^{-1} at 0.20 ± 0.01 hPa water vapor pressure (54.9 ± 5.9 % S wrt ice).

The lower actual ice yield than calculated is most likely due to deposition losses on non-extractible surfaces of the apparatus such as the caps of the flowtube or excess tubing inside the insulated chamber. Deposition of ambient humidity during sample extraction appears to be much lower than the losses present in the experimental setup. On average, the vapor deposition efficiency—that is the percent difference between the input and exhaust water vapor concentration, presumed to be the percentage of water deposited as ice—was 46%. This value never deviated more than 8% over the course of all experiments. This is potentially a geometric constraint of the flowtube apparatus as this value did not appear to change with temperature, flow rate, nor experiment time.

The size of any individual crystal was too small to reliably determine crystal morphology with nondestructive methods as the entire crystal yield was thinly coated over the interior surface of the flowtube (approximately 785 cm^2). This produced an ice coating that was typically less than 1 mg cm^{-2} and often not evenly distributed across the surface of the flowtube. While true morphology could not rigorously be determined, ice deposits where crystal growth was quicker along with areas with needle-like structures were observed.

3.2 Gas-Ice Partitioning Coefficients

To establish background signal during uptake experiments, ice crystals were grown in the flowtube from pure LC/MS grade water in three separate experiments at -20°C without organic gases. The signals in the ice blanks and clean denuder extract were in the same range as analytical blanks, which were all below detection limits. This demonstrates that no measurable contamination occurred during crystal growth or sample extraction.

At -20°C ($3.949 \times 10^{-3} \text{ K}^{-1}$), all compounds showed a $K < 1$. At lower temperatures, the K for all compounds increased except for MVK. This matches the expected behavior for exothermic deposition processes. Table 1 shows the calculated values for K at each temperature while Figure 2 plots these values against each other as a van't Hoff plot. Values of $K > 1$ or $\ln(K) > 0$ indicate net uptake of the compound into the ice phase for a system with equal volumes of gas and ice. Conversely, values of $K < 1$ or $\ln(K) < 0$ indicate negligible uptake and that the compound favors remaining in the gas phase for a system with equal volumes of gas and ice. At -30°C ($4.112 \times 10^{-3} \text{ K}^{-1}$), formaldehyde is favorable to deposit to the ice phase while acetaldehyde reaches conditions where K is close to 1 and the amount deposited to the ice phase and that remaining in the vapor phase are roughly equal. While formaldehyde is still mainly present in the gas phase at -20°C ($3.949 \times 10^{-3} \text{ K}^{-1}$), deposition of formaldehyde in the ice phase is favored from about -30°C ($4.112 \times 10^{-3} \text{ K}^{-1}$), while at this temperature acetaldehyde reaches conditions where K is close to 1 and thus the amount deposited in the ice phase and the amount remaining in the gas phase are approximately equal. At -40°C ($4.288 \times 10^{-3} \text{ K}^{-1}$), glyoxal and diacetyl also approach the point where K is approximately equal to 1, while formaldehyde, acetaldehyde, acetone, and propionaldehyde preferentially deposit in the ice phase. Formaldehyde is the only species, however, that strongly favors the ice phase with a K value in the order of 10^2 , while the other values are still around 10^0 or far below. Formaldehyde has the highest ice-partitioning coefficients in this study; the potential reasons for this are discussed further in section 3.5. Formaldehyde is thought to be the main source of OH radicals in the upper troposphere (Cooke et al., 2010; Fried et al., 2016). It then is likely that this ice uptake could be a significant influence on OH radical formation in the upper troposphere.

Table 1. Average Gas-Ice partitioning coefficients from uptake experiments at different temperatures

	<i>K</i> at –20 °C	<i>K</i> at –30 °C	<i>K</i> at –40 °C
MVK	$(2.21 \pm 1.23) \times 10^{-2}$	$(2.05 \pm 2.08) \times 10^{-3}$	$(9.01 \pm 8.26) \times 10^{-3}$
Acetaldehyde	$(1.27 \pm 0.35) \times 10^{-1}$	0.98 ± 1.37	3.10 ± 1.62
Acetone	$(1.87 \pm 0.54) \times 10^{-1}$	$(2.92 \pm 3.84) \times 10^{-1}$	2.14 ± 2.36
Benzaldehyde	$(7.68 \pm 2.86) \times 10^{-5}$	$(6.64 \pm 4.98) \times 10^{-4}$	$(1.43 \pm 1.14) \times 10^{-2}$
Camphor	$(5.08 \pm 0.70) \times 10^{-4}$	$(6.99 \pm 7.67) \times 10^{-3}$	$(5.97 \pm 4.25) \times 10^{-2}$
Diacetyl	$(3.69 \pm 1.13) \times 10^{-3}$	$(3.17 \pm 2.94) \times 10^{-2}$	1.33 ± 1.10
Formaldehyde	$(2.10 \pm 0.62) \times 10^{-1}$	$(1.38 \pm 1.98) \times 10^1$	$(1.03 \pm 0.63) \times 10^2$
Glyoxal	$(9.01 \pm 1.22) \times 10^{-3}$	$(6.78 \pm 2.45) \times 10^{-2}$	1.05 ± 1.54
Hydroxyacetone	$(1.64 \pm 0.23) \times 10^{-3}$	$(2.34 \pm 3.12) \times 10^{-2}$	$(3.55 \pm 4.63) \times 10^{-1}$
Methacrolein	$(3.94 \pm 1.89) \times 10^{-3}$	$(1.15 \pm 1.43) \times 10^{-2}$	$(2.10 \pm 3.06) \times 10^{-1}$
Methylglyoxal	$(7.29 \pm 2.99) \times 10^{-3}$	$(5.61 \pm 3.65) \times 10^{-2}$	$(3.95 \pm 3.40) \times 10^{-1}$
Nopinone	$(9.28 \pm 2.39) \times 10^{-6}$	$(1.10 \pm 0.67) \times 10^{-4}$	$(1.65 \pm 2.44) \times 10^{-3}$
Norcamphor	$(4.32 \pm 2.07) \times 10^{-5}$	$(9.05 \pm 2.72) \times 10^{-5}$	$(6.15 \pm 7.59) \times 10^{-3}$
Propionaldehyde	$(1.38 \pm 1.25) \times 10^{-1}$	$(2.11 \pm 2.30) \times 10^{-1}$	2.93 ± 3.23

Every measured species except for MVK displays a strong correlation of $\ln(K)$ with inverse temperature and can likely be exclusively described by thermodynamic sorption. Furthermore, the uptake of these species can almost exclusively ~~be~~ attributed to codeposition with water vapor during crystal growth as sorption on nongrowing crystals has been demonstrated to be insignificant or completely reversible for almost all chemical species studied. This specifically includes acetone, acetaldehyde, formaldehyde, and benzaldehyde (Fries et al., 2006; Hudson et al., 2002; Roth et al., 2004; Winkler et al., 2002). This observation of strong correlations with inverse temperature could indicate that *K* is controlled by transport, specifically if analyte transport is limited by accommodation at the ice-air interface (Davidovits et al., 2006; Jayne et al., 1991).

MVK however shows a weak negative trend with inverse temperature with a nonsignificant correlation. The absence of this correlation for MVK complicates this view of *K* controlled by transport. However, this could be explained by kinetic control resulting from transport phenomena occurring in either the gas or solid phases, i.e. processes that change the rates of transport of MVK relative to water vapor rather than a *K* that is controlled by an equilibrium established between MVK and ice. However, without sufficient evidence for a mechanism of kinetically controlled transport, the measurements of *K* here will be interpreted using equilibrium thermodynamics. While

outside the scope the current study, a kinetic explanation could be explored through theoretical calculations such as those found in Conklin and Bales (1993) or Reif (1965).

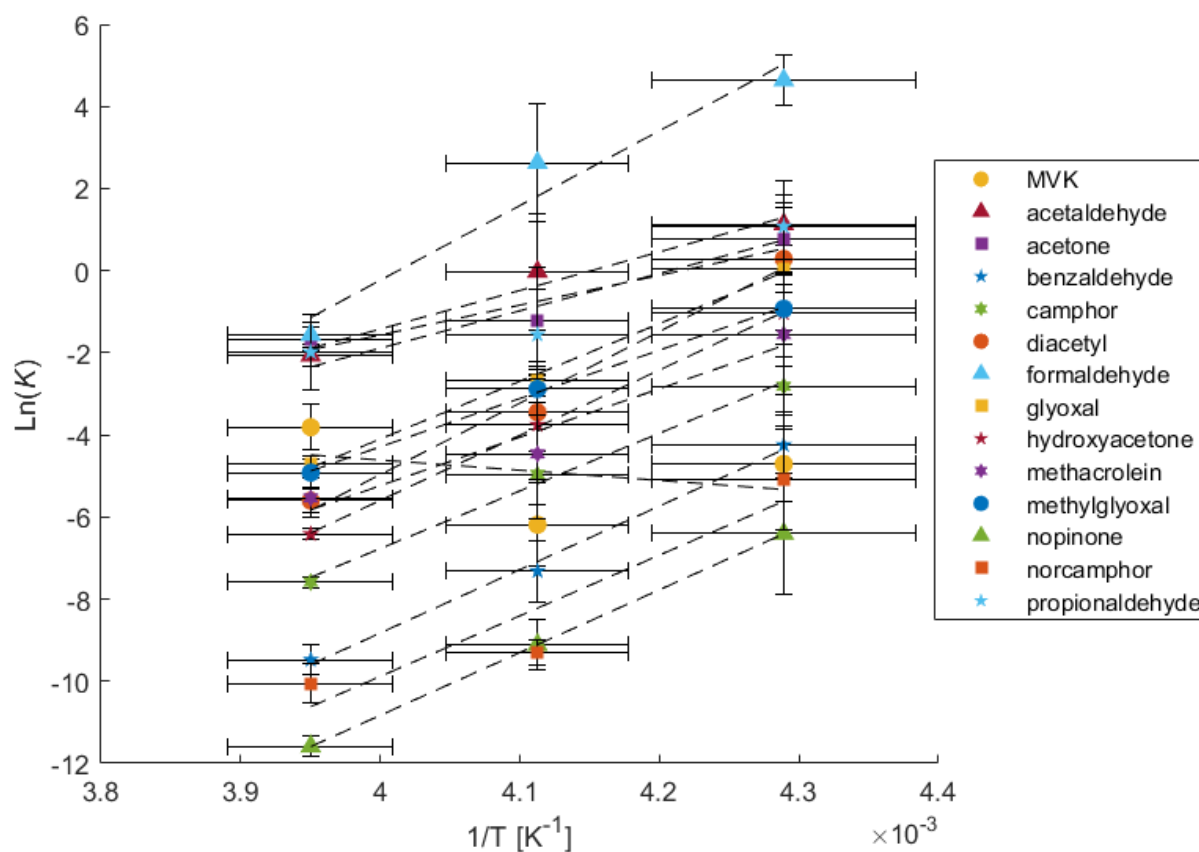


Figure 2. Van't Hoff plot of inverse temperature (K^{-1}) against the natural log of the calculated partitioning coefficient K (unitless)

3.3 Thermodynamic Results

The Van't Hoff analysis of uptake can be used to estimate the enthalpy and entropy of thermodynamic sorption. Tables 2 and 3 apply the thermodynamic analysis from Eqs. 6 and 7 to the data given in Table 1 and the linear regressions seen in Figure 1. Table 2 provides the ΔG values produced by applying Eq. 6 the partitioning coefficients given in Table 1. Table 3 contains the slopes, intercepts, and regression coefficients (r^2) for the linear

regressions in Figure 1 as well as the calculated uptake enthalpy (ΔH) and uptake entropy (ΔS) produced by Eq. 7.

In Table 2, a $\Delta G > 0$ indicates unfavorable uptake of the species into the ice phase while $\Delta G < 0$ indicates favorable

uptake into the ice phase for a system with equal volumes of gas and ice. At -20 °C, it is not favorable for uptake into the ice phase to occur for any species. At -30 °C, it is thermodynamically favorable for formaldehyde to be taken into the ice phase. At -40 °C, glyoxal, diacetyl, formaldehyde, acetaldehyde, acetone, and propionaldehyde are thermodynamically favorable to be taken into the ice phase. Interpolating for these species, it becomes favorable to deposit acetaldehyde, acetone, and propionaldehyde into the ice phase between -32 °C and -35 °C while formaldehyde begins to deposit at -24.3 °C. Both glyoxal and diacetyl deposit at approximately -40 °C. Since cirrus clouds often can occur at temperatures such as -60 °C and lower, this data implies that uptake at those temperatures could significantly affect the availability of these species. With these carbonyls being the typical source of atmospheric OH radicals, this would significantly reduce the availability of OH radicals within cirrus clouds.

The other species—MVK, benzaldehyde, camphor, hydroxyacetone, methacrolein, methlyglycolal, nopinone, and norcamphor—were unfavorable to deposit into the ice phase under any of the conditions studied here. Extrapolating based on the linear regression in Table 3, the estimated temperature below which it is favorable to deposit the species (excepting MVK) is presented in Table 2. For these species, they would presumably become favorable to deposit into the ice phase within the range of -43 to -61 °C, which is within the natural range for cirrus clouds. With MVK having both a poor regression ($r^2 = 0.1235$) and nonexothermic behavior, the temperature at which $\Delta G = 0$ cannot be meaningfully extrapolated.

Table 2. Calculated ΔG of uptake at different temperatures.

Temperature (°C)	ΔG (kJ mol ⁻¹)			Calculated T where $\Delta G = 0$ (°C)
	-20	-30	-40	
MVK	8.0	12.5	9.1	–
Acetaldehyde	4.3	0.1	-2.2	-32.2
Acetone	3.5	2.5	-1.5	-35.4
Benzaldehyde	19.9	14.8	8.2	-54.3
Camphor	16.0	10.0	5.5	-49.9

Diacetyl	11.8	7.0	−0.6	−39.6
Formaldehyde	3.3	−5.3	−9.0	−24.3
Glyoxal	9.9	5.4	−0.1	−40.1
Hydroxyacetone	13.5	7.6	2.0	−43.4
Methacrolein	11.7	9.0	3.0	−47.3
Methylglyoxal	10.4	5.8	1.8	−43.9
Nopinone	24.4	18.4	12.4	−60.7
Norcamphor	21.2	18.8	9.9	−56.5
Propionaldehyde	4.2	3.1	−2.1	−34.8

415 **Table 3. Slopes ($\Delta H/R$), intercepts ($\Delta S/R$), and regression coefficients (r^2) of regression lines from Figure 1, calculated uptake enthalpy (ΔH), and uptake entropy (ΔS).**

	$-\Delta H/R$ (K)	$\Delta S/R$	r^2	ΔH (kJ mol ^{−1})	ΔS (J mol ^{−1} K ^{−1})
MVK	−2486.8	5.33	0.1235	20.68	44.4
Acetaldehyde	9392.4	−38.99	0.9672	−78.09	−324.2
Acetone	7256.3	−30.59	0.8972	−60.33	−254.4
Benzaldehyde	15452.5	−70.64	0.9941	−128.48	−587.3
Camphor	14040.3	−62.93	0.9934	−116.74	−523.2
Diacetyl	17426.7	−74.67	0.9830	−144.89	−620.9
Formaldehyde	18197.2	−73.02	0.9508	−151.30	−607.1
Glyoxal	14049.0	−60.30	0.9960	−116.81	−501.3
Hydroxyacetone	15872.3	−69.09	0.9997	−131.97	−574.4
Methacrolein	11804.2	−52.45	0.9450	−98.15	−436.1
Methylglyoxal	11766.5	−51.36	0.9987	−97.83	−427.0
Nopinone	15285.4	−71.97	1.0000	−127.09	−598.4
Norcamphor	14765.6	−68.95	0.8752	−122.77	−573.2
Propionaldehyde	9111.8	−38.34	0.8690	−75.76	−318.7

All linear regressions calculated in Table 3 except for MVK have r^2 greater than 0.86 which indicate good linearity. The weakest regressions include norcamphor, propionaldehyde, and acetone which are between 0.869 and 0.897 while all the other regressions are above 0.945; those above 0.993 are benzaldehyde, camphor, glyoxal, hydroxyacetone, methylglyoxal, and nopinone. It can then be concluded that the gas-ice partitioning of all the species studied here except for MVK can be explained by the thermodynamic parameters of bulk uptake. The calculated ΔH and ΔS are then accurate descriptions of the thermodynamic process for these species' uptake in the ice phase. ΔH and ΔS are negative for all species except MVK and are within the ranges of -60 to -151 kJ mol^{-1} and -254 to -621 $\text{J mol}^{-1} \text{K}^{-1}$ respectively. These values indicate that at increasingly colder temperatures the uptake of all these species becomes more efficient and uptake decreases at warmer temperatures.

For MVK, since the linearity of the regression is poor, thermodynamic discussion of its measured partitioning coefficients is limited. Taking the calculated ΔH and ΔS at face value suggests that MVK behaves endothermically, and that uptake decreases at colder temperatures. This positive correlation with temperature has also been seen in the uptake of C_1 – C_4 -alkanols (Huffman and Snider, 2004), which is attributed to weakened water-water bonding when incorporated into ice due to supposed hydrogen bonding. MVK as a ketone is a hydrogen bond acceptor, as are the other ketones and aldehydes in this study, so this weak correlation is unlikely exclusively related to hydrogen bonding effects. More importantly, MVK is demonstrated to efficiently undergo functionalization and oligomerization in the aqueous phase through photooxidation (Renard et al., 2014). It is then a possibility that this photodegradation process is the main cause of the weak correlation that MVK has with inverse temperature. However, other similar compounds such as glyoxal and methacrolein also have demonstrated efficient functionalization and oligomerization through photooxidation but they do not exhibit the same poor regression as MVK. As an enone, MVK has also been observed to undergo unimolecular tautomerization, forming 2-hydroxybutadiene, however this involves high temperatures or intense UV (Couch et al., 2021). Additionally, almost all ketones are capable of tautomerization, not just MVK. Assuming that MVK's anomalous behavior is not due to its reactive properties obscuring observation, an explanation for this behavior could be found in its water-binding properties. While there are four observed conformational isomer adducts of MVK with water, the antiperiplanar conformation of MVK is preferred and is then stabilized by a network of two intermolecular interactions. These are the $\text{O} - \text{H} \cdots \text{O}$ hydrogen bond between the MVK oxygen and the water H atoms, and the second hydrogen bond $\text{C} - \text{H} \cdots \text{O}$ established between the water oxygen atom and one H atom from the methyl group (Cabezas et al., 2022).

If there's a change in the pattern of available hydrogen bonds, possibly incurred by the ice-growth kinetics that determine the principal facet, this could make MVK's preferred adduct conformation less favorable for accommodating to the ice surface. This would impose an energetic barrier to uptake which could explain MVK's anomalous behavior.

450

3.4 Entropy-Enthalpy Compensation

Plotting the calculated ΔH and ΔS , as seen in Figure 3, demonstrates an apparent entropy-enthalpy compensation (EEC) effect, where ΔH scales proportionately with ΔS . This relationship appears to also extend to the
455 calculated ΔH and ΔS for MVK. This form of linear correlation between ΔS and ΔH , where it arises for a series of homologous compounds employed in a process, is referred to as the strong form of EEC (Sharp, 2001). This compensation effect appears to have good linearity with an r^2 of 0.9809 with no noticeable outliers with a compensation temperature (i.e. slope; $T_c = d\Delta H/d\Delta S$) of 235.5 K. EEC however has been known to arise as a statistical artefact with high r^2 and is often controversial (Grunwald and Steel, 1995; Krug et al., 1976; Leffler, 1955;
460 Leung et al., 2008; Liu and Guo, 2001; Moulik et al., 2019; Pan et al., 2015; Sharp, 2001). This is because methods such as van't Hoff analysis are indirect and do not measure ΔH and ΔS independently. Thus, for measurements on a limited temperature range, true observation of ΔH and ΔS can be obscured by trivial correlation arising from larger errors in determining ΔH than ΔG rather than some extra-thermodynamic mechanism of EEC (Sharp, 2001). Additionally, van't Hoff analysis assumes that the enthalpy change relative to the reference-state enthalpy change is
465 negligible (i.e., the heat capacity change is negligible). This may be invalid for an experimental temperature which may be significantly different from the reference-state enthalpy (Leung et al., 2008). Therefore, it is critical to evaluate EEC occurrence through statistical methods. For brevity, many of the specifics of this analysis has been moved to the Supplementary Materials under Section S1. The most relevant aspects and conclusions are presented here.

470

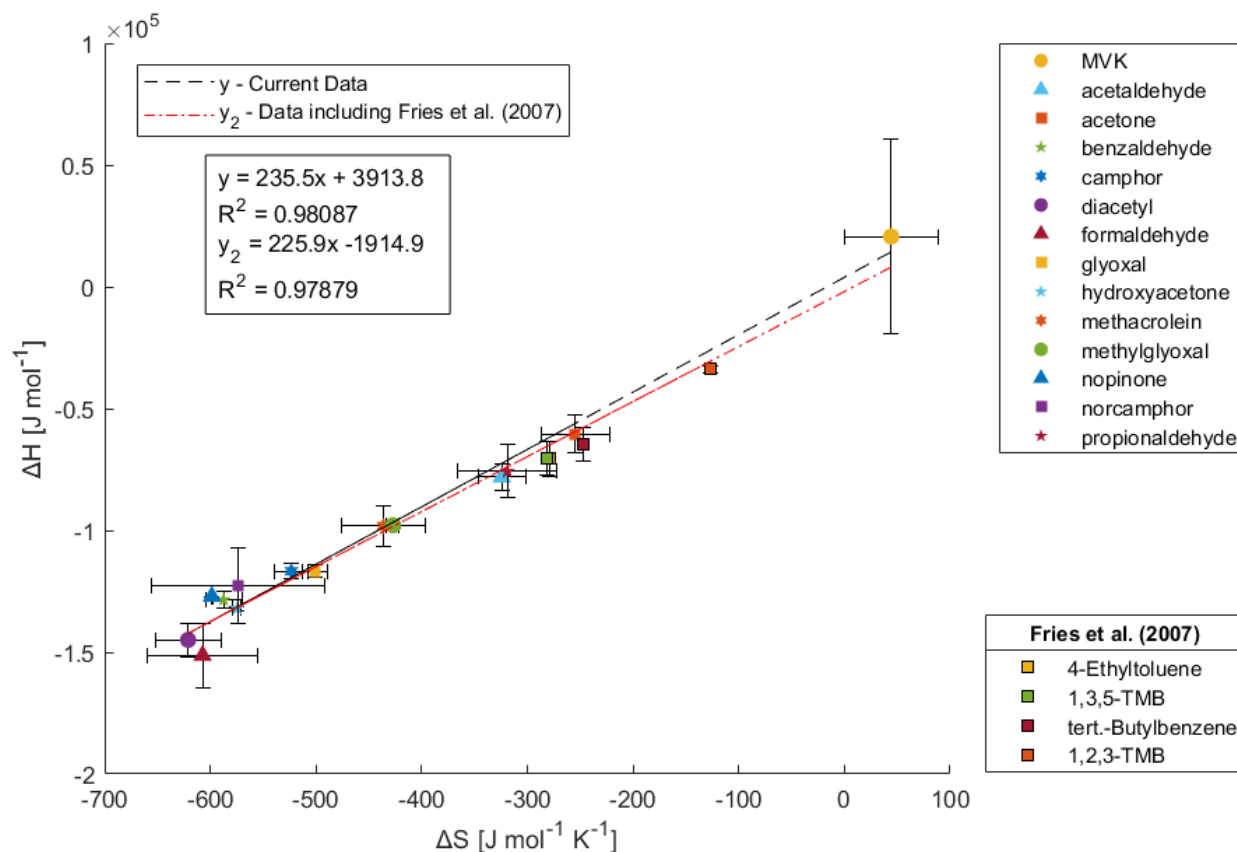


Figure 3. Enthalpy versus entropy plot using the ΔH and ΔS determined from the Van 't Hoff plots in Figure 2

To rigorously investigate EEC, the simple statistical verification of EEC provided by Griessen and Dam (2021) is applied to this data. The calculated dimensionless coalescence location parameter and Compensation Quality Factor pair (k , CQF) for this data is $(-0.278, 0.062)$; which when plotted on Griessen and Dam's confidence contours, lies outside the 99% confidence contour for $n = 12$ (This dataset is $n = 14$). This indicates that there is 99% confidence that the EEC seen here is not of statistical origin. For good measure, if the data from Fries et al. (2007) is included in the (k , CQF) calculation, the calculated (k , CQF) pair is $(-1.264, 0.205)$ and lies even further from the 99% confidence contour for $n = 12$ (This dataset is $n = 18$). From this statistical analysis, it can then be rigorously stated that the EEC seen in gas-ice partitioning is not artifactual in origin and likely has an extra-thermodynamic mechanism.

While an initial explanation of this mechanism might stem from a discussion on specific functional group-driven interactions, the appearance of this EEC effect includes aromatic hydrocarbons in addition to the ketones and aldehydes studied here. This could indicate that instead there may be weak, nonspecific supramolecular interactions. A few such explanations for EEC that are applicable to gas-ice equilibrium have been discussed in literature. Firstly, EEC due to solvation effects (i.e. solvent reorganization) are commonly discussed (Dragan et al., 2017; Leung et al., 2008; Lumry and Rajender, 1970; Pan et al., 2015). These discussions often center around the concept that any process that changes the free volume of nearby liquid water is inherently compensatory due to “structure making” and “structure breaking” of hydration shells. This explanation of EEC for gas-ice partitioning during depositional ice growth implies a surface liquid layer or quasi-liquid layer behavior. Indeed, there is already evidence for this as Huffman and Snider (2004) observe that at temperatures colder than approximately -20°C there is overlap with models describing uptake into a surface liquid layer and previous uptake studies also use aqueous film models to account for SO_2 capture (Valdez et al., 1989).

Regardless of the specific mechanism of the EEC in this system, its presence does support (but does not necessarily prove) that there is a single source of additivity for the series of compounds studied (Lumry, 1995); i.e. a single thermodynamic component that controls the uptake process. Contrarily, there are also those who believe that EEC is not explainable and that it is an arbitrary phenomenon that arises from narrow free energy ranges (Moulik et al., 2019).

3.5 Partitioning Coefficients versus Heat of Vaporization and Molar Mass

The values for K and $\ln K$ at -20°C were regressed with several physiochemical properties, specifically molar mass (MM), HPLC retention time (RT), vapor pressure (P_{vap} at 25°C), heat of vaporization ($\Delta H_{\text{vap}}^{\circ}$) (Chickos et al., 1995), van der Waals volume (Zhao et al., 2003), and Henry solubility (Sander, 2023). These regressions were also made for K and $\ln K$ at -30 and -40°C , however all the notable trends are the same. Further, regressions were made with uptake ΔH and ΔG , however the only significant correlations were from $\ln K$ against $\ln P_{\text{vap}}$, MM, $\Delta H_{\text{vap}}^{\circ}$, and van der Waals volume ($n = 14$, $r^2 = 0.749, 0.737, 0.711, 0.702$ respectively). $\ln P_{\text{vap}}$ positively correlates while the rest of these properties all correlate negatively with $\ln K$, indicating a relationship where larger compounds have lower uptake into ice and higher vapor pressures indicate more uptake. These correlations for MM and $\Delta H_{\text{vap}}^{\circ}$ at -20

°C are displayed in Figure 4 while the same for –30 and –40 °C are provided in the Supplemental Material as Figures S3 and S4. [Additional correlations are provided in the Supplemental Material as Figures S5-S8.](#) The higher r^2 for the regression against MM suggests that molecular size is the main contributor for uptake of carbonyls as opposed to aqueous solubility or hydrogen bonding potential. The ability for ketones and aldehydes to hydrogen bond is limited as they are only capable of being bond acceptors. If hydrogen bonding between analyte and water played a significant role in the uptake process, then it would be expected that Henry solubilities would be more relevant contributors. Since carbonyls are unable to form hydrogen bonds between themselves, it's likely that the correlation from ΔH_{vap}^0 is driven mostly from molecular size, as ΔH_{vap}^0 is a property describing a pure substance. In this case, MM and ΔH_{vap}^0 positively correlate with an r^2 of 0.746 so their similar regressions are proxies of each other. Further, the residuals of the regressions for both properties are very similar. Almost all compounds stay on the same side of both regressions, i.e. few compounds change between positive and negative residuals. The exceptions to this are MVK, methylglyoxal, and hydroxyacetone. MM and van der Waals volume also positively correlate with an r^2 of 0.987, so van der Waals volume is considered a proxy for MM. $\ln P_{vap}$ however negatively correlates with MM with an r^2 of 0.778, so $\ln P_{vap}$ can also be considered a collinear factor to MM.

The negative relationship of uptake with molecular size and positive relationship with vapor pressure is a unique finding that may seem counterintuitive if not considering inclusion into the ice lattice structure. One might expect that compounds with a higher affinity for the gas phase will remain in the gas phase and therefore have lower uptake coefficients. However, the reverse is observed. Compounds with higher vapor pressures and lower masses are more readily taken into the ice phase. If in order to be taken into the ice phase, a compound must be incorporated into the ice crystal lattice structure, then this trend becomes more reasonable. Smaller compounds may induce less deviation in lattice structure relative to the preferred ice crystal structure. It may then be energetically less favorable for a larger compound to fit into the ice crystal as it forces a larger crystallographic defect. This trend might not be expected if analytes are phase separated from the ice crystal in grain boundaries. Other studies have suggested that simple organics like formaldehyde are incorporated into the ice crystal volume under similar freezing conditions that produces snow (Perrier et al., 2002). This trend has been similarly hypothesized by Jost et al. (2017) for rime growth ice, but recent studies have not found this trend in rime growth ice nor bulk phase liquid freezing (Borchers et al., 2024; Gautam et al., 2024; Seymore et al., 2024). Huffman and Snider (2004) did not observe any specific dependence of uptake on compound saturation partial pressure nor molecular mass for acetone, toluene, or the C_{1-}

C₃ alkanols, but they observed a similar negative correlation with ΔH_{vap}^0 as also seen here. Fries et al. (2007) did not observe any trends between the physical properties of aromatic hydrocarbons and their uptake. An alternative explanation could be that the preferential uptake of smaller compounds is due to possible mesoporous conditions on the ice surface; i.e. pores that develop on the ice surface prevent the accommodation of larger compounds which are sterically inhibited from entering small pores.

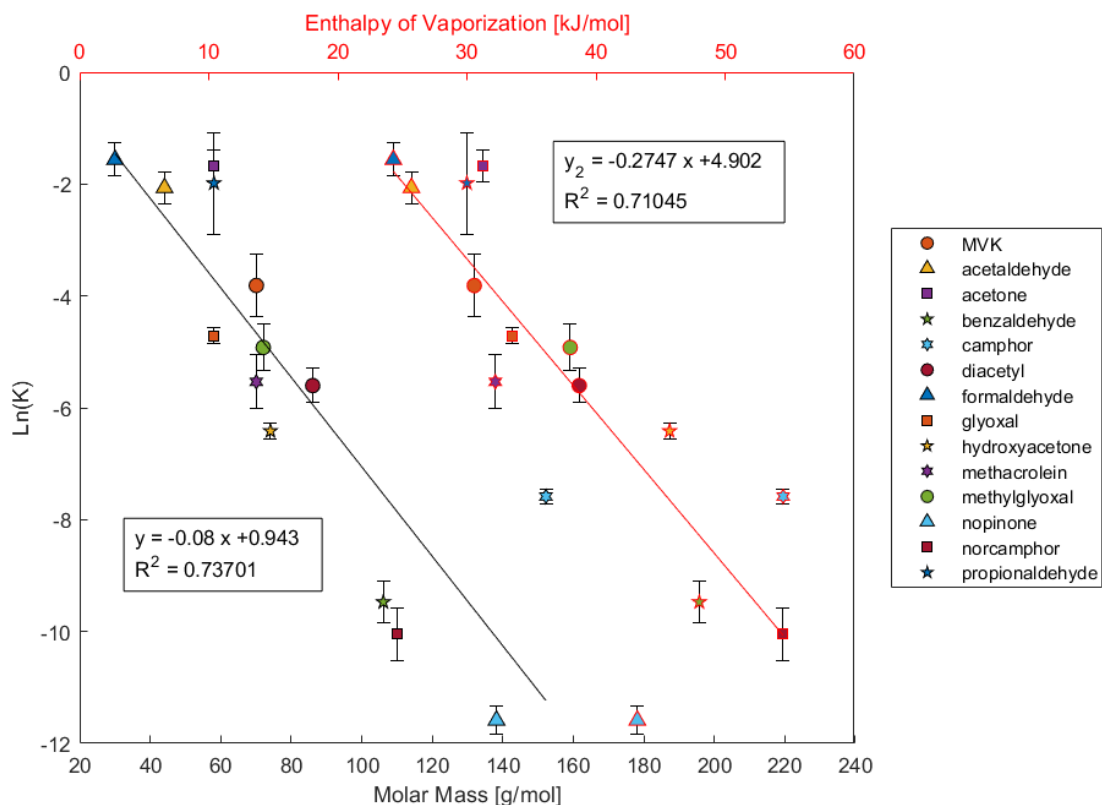


Figure 4. Scatterplot of $\ln(K)$ at -20°C versus the heat of vaporization (red line) and molar mass (black line).

4 Conclusions

The uptake of carbonyls by ice crystals grown by deposition was studied at temperatures between -20°C and -40°C . Ice was grown from the vapor phase in the presence of gas phase carbonyls using a flowtube apparatus where ice saturation was controlled for a realistic saturation prevalent in natural cirrus clouds. Uptake of the carbonyl compounds from the gas phase during crystal growth was observed. Performing this experiment at

different temperatures allowed for the entropy and enthalpy of uptake to be determined. A linear correlation between ΔS and ΔH arose which was statistically validated and determined with 99% confidence that the EEC seen is not a statistical artifact. This compensation behavior could be an indication of a surface liquid layer or quasi-liquid layer behavior involved in this process; or it could also indicate a single dominant influence on a compound's uptake. The most significant chemical properties correlated with uptake were identified to be molecular size and vapor pressure. Their relationship to uptake is indicative of incorporation into the ice crystal structure, as smaller compounds have higher observed uptakes.

In agreement with previous studies, these results indicate that deposition into the ice phase is a possible uptake process for organic compounds in cirrus clouds. Since ice growth in the troposphere at low temperatures is a major contributor to precipitation, in-cloud scavenging is a plausible explanation for the occurrence of organics in fresh snow (Roth et al., 2004; Su et al., 2021). Therefore, interactions of ice and organic compounds can influence atmospheric transport and removal of those compounds from the atmosphere by deposition. The partitioning coefficients observed here are however below—by at least 3 orders of magnitude—the $10 \text{ mol m}^{-3} \text{ Pa}^{-1}$ threshold from Crutzen and Lawrence (2000) to be considered a substantial atmospheric removal process. Importantly, the partitioning of these compounds to the ice phase are governed in part by the volume ratio of the partitioning phases and may be less relevant in situations where the amount of ice is magnitudes smaller than the amount of gas, which describes nearly all natural cloud conditions (Brimblecombe and Dawson, 1984). Specifically, to appreciably accumulate a significant fraction of a compound from the gas phase, a large K is needed in order to overcome the difference in ice and air, likely a $\ln(K) > 10$.

Compared to the well-studied uptake of HNO_3 , the uptake of most species studied here are 2-3 orders of magnitude lower while acetaldehyde, acetone, formaldehyde, and propionaldehyde may be considered in comparable range (Von Kuhlmann and Lawrence, 2006; Zondlo et al., 1997). Notably, as these species are relevant as significant sources of OH radicals in the upper troposphere (Cooke et al., 2010; Fried et al., 2016), it then is likely that this ice uptake could be a significant influence on OH radical formation in the upper troposphere at temperatures less than the range studied here, notably -60°C where the extrapolated uptake could reach $\ln(K) > 10$.

For comparative reference, the partitioning coefficients reported here can be converted from dimensionless coefficients to $\text{mol m}^{-3} \text{ Pa}^{-1}$ by dividing by RT , which is provided in the supplement. Further, the uptake coefficients

for carbonyls are on average smaller than those for aromatic hydrocarbons studied by (Fries et al., 2007), which have already been estimated to be removed primarily by photochemical processes rather than ice phase scavenging. While this removal process cannot be considered substantial in terms of mass transport, it may be relevant as an influence on vertical tracer transport or OH radical formation.

These measurements are exclusively a description of the gas to ice solid solution equilibrium and neglect investigation of gas to liquid or liquid to ice equilibrium. Critically, the measurements here could be influenced by liquid water condensation within the Flowtube. Provided some regions of the glass substrate are clean and free from ice nucleating sites, some liquid phase water could condense directly to the substrate and then freeze thus competing with the diffusional growth ice. Additionally, some liquid water could condense into droplets within the gas stream and then impact on the substrate thereby contributing to the deposited ice via riming. These alternate modes of freezing are unlikely to occur under these conditions as the clean carrier/dilution gas has virtually no nucleating particles for liquid droplet condensation and the glass Flowtube substrate is ideal for facilitating dendritic ice crystal growth (Chen et al., 2020). However, the presence of liquid water condensation within the Flowtube could be an alternative explanation to the observed exothermic uptake trends, assuming that Henry's law uptake into the liquid phase increases with decreasing temperature below 273 K. If this were the case, Henry solubilities should be the dominate factor controlling uptake and it would also be expected that more water-soluble species like glyoxal would have much higher uptake coefficients than less water-soluble species like formaldehyde. Neither of these are observed here so it can be concluded that liquid water condensation within the Flowtube is unlikely to have significantly influenced the present measurements.

These partitioning coefficients also do not directly describe whether a compound is actually incorporated into the ice crystal lattice or if it phase separates into crystal grain boundaries, but only its uptake into the bulk phase. However, the negative correlation of molecular size and uptake may suggest incorporation into the ice crystal lattice or void space. It is also difficult to say if this data describes uptake into a liquid solution phase that coexists with ice, but the observed compensation effect may insinuate its presence. While the measurements here are for multicomponent mixtures of compounds, single component uptake is likely the same, which is also supported by Huffman and Snider (2004).

Further investigation to determine the contribution of liquid layer influence should focus on measuring on ice-specific surface area and the volume of solution associated with the liquid layer. Additionally, similar experiments with other families of compounds are required to better understand the root of the compensation effect seen here. Crystallographic analysis of this data may also yield more information about the ice uptake process. With more investigation to reveal the main contributors of additivity, it seems possible that the EEC seen here could be used to help generalize descriptions of the uptake process in models.

Acknowledgements

This work was funded by the Deutsche Forschungsgemeinschaft (DFG, German Research Foundation) – TRR 301 – Project-ID 428312742.

This work was supported by the Max Planck Graduate Center with the Johannes Gutenberg University of Mainz (MPGC) as well as by internal funding from the Max Planck Institute for Chemistry (MPIC). We would also like to acknowledge the mechanical workshop of the Johannes Gutenberg University Institute of Atmospheric Physics (JGU-IPA) and the glass workshop of the Max Planck Institute for Polymer Research (MPIP) for their technical expertise and contributions.

Special thanks to Jan Wallner for his contributions testing the experimental setup.

Author Contributions

JS, MS, AT, SM participated in designing the experiments; JS, AT, SM participated in constructing the experimental apparatus; JS prepared the solutions for experiments, performed the experiments, and collected the samples; JS, CB conducted the analytical measurements; JS analyzed the data and wrote the manuscript draft; JS, MS, AT, CB, TH reviewed and edited the manuscript.

Competing Interests

The contact author has declared that none of the authors has any competing interests

References

- 630 Abbatt, J. P. D., Bartels-Rausch, T., Ullerstam, M., and Ye, T. J.: Uptake of acetone, ethanol and benzene to snow and ice: effects of surface area and temperature, *Environmental Research Letters*, 3, 045008, <https://doi.org/10.1088/1748-9326/3/4/045008>, 2008.
- Bartels-Rausch, T., Jacobi, H. W., Kahan, T. F., Thomas, J. L., Thomson, E. S., Abbatt, J. P. D., Ammann, M., Blackford, J. R., Bluhm, H., Boxe, C., Domine, F., Frey, M. M., Gladich, I., Guzmán, M. I., Heger, D., Huthwelker, T., Klán, P., Kuhs, W. F., Kuo, M. H., Maus, S., Moussa, S. G., McNeill, V. F., Newberg, J. T., Pettersson, J. B. C., Roeselová, M., and Sodeau, J. R.: A review of air-ice chemical and physical interactions (AICI): Liquids, quasi-liquids, and solids in snow, *Atmos Chem Phys*, 14, 1587–1633, <https://doi.org/10.5194/ACP-14-1587-2014>, 2014.
- 635 Behr, P., Terziyski, A., and Zellner, R.: Acetone adsorption on ice surfaces in the temperature range $T = 190\text{--}220\text{ K}$: Evidence for aging effects due to crystallographic changes of the adsorption sites, *Journal of Physical Chemistry A*, 110, 8098–8107, <https://doi.org/10.1021/JP0563742/ASSET/IMAGES/LARGE/JP0563742F00011.JPEG>, 2006.
- Borchers, C., Seymore, J., Gautam, M., Dörholt, K., Müller, Y., Arndt, A., Gömmers, L., Ungeheuer, F., Szakáll, M., Borrmann, S., Theis, A., Vogel, A. L., and Hoffmann, T.: Retention of α -pinene oxidation products and nitro-aromatic compounds during riming, *Atmos Chem Phys*, 24, 13961–13974, <https://doi.org/10.5194/ACP-24-13961-2024>, 2024a.
- 645 Borchers, C., Seymore, J., Gautam, M., Dörholt, K., Müller, Y., Arndt, A., Gömmers, L., Ungeheuer, F., Szakáll, M., Borrmann, S., Theis, A., Vogel, A. L., and Hoffmann, T.: Retention of α -pinene oxidation products and nitro-aromatic compounds during riming, <https://doi.org/10.5194/egusphere-2024-1443>, 2024b.
- Brimblecombe, P. and Dawson, G. A.: Wet removal of highly soluble gases, *J Atmos Chem*, 2, 95–107, <https://doi.org/10.1007/BF00127265/METRICS>, 1984.
- 650 Cabezas, C., Juanes, M., Saragi, R. T., Lesarri, A., and Peña, I.: Water binding to the atmospheric oxidation product methyl vinyl ketone, *Spectrochim Acta A Mol Biomol Spectrosc*, 270, 120846, <https://doi.org/10.1016/J.SAA.2021.120846>, 2022.
- Chen, G., Kong, W., Wang, L., and Wang, F.: On the experimental and theoretical model for ice crystal characteristics near a substrate, *Int J Heat Mass Transf*, 152, 119462, <https://doi.org/10.1016/J.IJHEATMASTRANSFER.2020.119462>, 2020.
- 655 Chickos, J. S., Hosseini, S., and Hesse, D. G.: Determination of vaporization enthalpies of simple organic molecules by correlations of changes in gas chromatographic net retention times, *Thermochim Acta*, 249, 41–62, [https://doi.org/10.1016/0040-6031\(95\)90670-3](https://doi.org/10.1016/0040-6031(95)90670-3), 1995.
- Comstock, J. M., Ackerman, T. P., Turner, D. D., Comstock, J. M., Ackerman, T. P., and Turner, D. D.: Evidence of high ice supersaturation in cirrus clouds using ARM Raman lidar measurements, *Geophys Res Lett*, 31, 11106, <https://doi.org/10.1029/2004GL019705>, 2004.
- Conklin, M. H. and Bales, R. C.: SO₂ uptake on ice spheres: Liquid nature of the ice-air interface, *Journal of Geophysical Research: Atmospheres*, 98, 16851–16855, <https://doi.org/10.1029/93JD01207>, 1993.
- 665 Conklin, M. H., Sommerfeld, R. A., Kay Laird, S., and Villinski, J. E.: Sulfur dioxide reactions on ice surfaces: implications for dry deposition to snow, *Atmospheric Environment. Part A. General Topics*, 27, 159–166, [https://doi.org/10.1016/0960-1686\(93\)90346-Z](https://doi.org/10.1016/0960-1686(93)90346-Z), 1993.
- Cooke, M. C., Utembe, S. R., Gorrotxategi Carbajo, P., Archibald, A. T., Orr-Ewing, A. J., Jenkin, M. E., Derwent, R. G., Lary, D. J., and Shallcross, D. E.: Impacts of formaldehyde photolysis rates on tropospheric chemistry, *Atmospheric Science Letters*, 11, 33–38, <https://doi.org/10.1002/ASL.251>, 2010.
- 670 Couch, D. E., Nguyen, Q. L. D., Liu, A., Hickstein, D. D., Kapteyn, H. C., Murnane, M. M., and Labbe, N. J.: Detection of the keto-enol tautomerization in acetaldehyde, acetone, cyclohexanone, and methyl vinyl ketone with a

novel VUV light source, *Proceedings of the Combustion Institute*, 38, 1737–1744, <https://doi.org/10.1016/J.PROCI.2020.06.139>, 2021.

675 Crutzen, P. J. and Lawrence, M. G.: The Impact of Precipitation Scavenging on the Transport of Trace Gases: A 3-Dimensional Model Sensitivity Study, *Journal of Atmospheric Chemistry*, 81–112 pp., 2000.

Davidovits, P., Kolb, C. E., Williams, L. R., Jayne, J. T., and Worsnop, D. R.: Mass Accommodation and Chemical Reactions at Gas–Liquid Interfaces, <https://doi.org/10.1021/cr040366k>, 2006.

680 Dekoutsidis, G., Groß, S., Wirth, M., Krämer, M., and Rolf, C.: Characteristics of supersaturation in midlatitude cirrus clouds and their adjacent cloud-free air, *Atmos Chem Phys*, 23, 3103–3117, <https://doi.org/10.5194/ACP-23-3103-2023>, 2023.

Diehl, K., Mitra, S. K., and Pruppacher, H. R.: A laboratory study of the uptake of HNO_3 and HCl vapor by snow crystals and ice spheres at temperatures between 0 and -40°C , *Atmos Environ*, 29, 975–981, 1995.

Dominé, F. and Thibert, E.: Mechanism of incorporation of trace gases in ice grown from the gas phase, *Geophys Res Lett*, 23, 3627–3630, <https://doi.org/10.1029/96GL03290>, 1996.

685 Dragan, A. I., Read, C. M., and Crane-Robinson, C.: Enthalpy–entropy compensation: the role of solvation, <https://doi.org/10.1007/s00249-016-1182-6>, 1 May 2017.

Ervens, B. and Kreidenweis, S. M.: SOA formation by biogenic and carbonyl compounds: Data evaluation and application, *Environ Sci Technol*, 41, 3904–3910, https://doi.org/10.1021/ES061946X/SUPPL_FILE/ES061946XSI20061123_082532.PDF, 2007.

690 Franz, T. P. and Eisenreich, S. J.: Accumulation of polychlorinated biphenyls and polycyclic aromatic hydrocarbons in the snowpack of Minnesota and Lake Superior, *J Great Lakes Res*, 26, 220–234, [https://doi.org/10.1016/S0380-1330\(00\)70688-5](https://doi.org/10.1016/S0380-1330(00)70688-5), 2000.

695 Fried, A., Barth, M. C., Bela, M., Weibring, P., Richter, D., Walega, J., Li, Y., Pickering, K., Apel, E., Hornbrook, R., Hills, A., Riemer, D. D., Blake, N., Blake, D. R., Schroeder, J. R., Luo, Z. J., Crawford, J. H., Olson, J., Rutledge, S., Betten, D., Biggerstaff, M. I., Diskin, G. S., Sachse, G., Campos, T., Flocke, F., Weinheimer, A., Cantrel, C., Pollack, I., Peischl, J., Froyd, K., Wisthaler, A., Mikoviny, T., and Woods, S.: Convective transport of formaldehyde to the upper troposphere and lower stratosphere and associated scavenging in thunderstorms over the central United States during the 2012 DC3 study, *Journal of Geophysical Research: Atmospheres*, 121, 7430–7460, <https://doi.org/10.1002/2015JD024477>, 2016.

700 Fries, E., Haunold, W., Jaeschke, W., Hoog, I., Mitra, S. K., and Borrmann, S.: Uptake of gaseous aromatic hydrocarbons by non-growing ice crystals, *Atmos Environ*, 40, 5476–5485, <https://doi.org/10.1016/J.ATMOSENV.2006.03.055>, 2006.

705 Fries, E., Starokozhev, E., Haunold, W., Jaeschke, W., Mitra, S. K., Borrmann, S., and Schmidt, M. U.: Laboratory studies on the uptake of aromatic hydrocarbons by ice crystals during vapor depositional crystal growth, *Atmos Environ*, 41, 6156–6166, <https://doi.org/10.1016/j.atmosenv.2007.04.028>, 2007.

Galeazzo, T., Aumont, B., Camredon, M., Valorso, R., Lim, Y. B., Ziemann, P. J., and Shiraiwa, M.: Secondary organic aerosols derived from intermediate-volatility n-alkanes adopt low-viscous phase state, *Atmos Chem Phys*, 24, 5549–5565, <https://doi.org/10.5194/ACP-24-5549-2024>, 2024.

710 Gautam, M., Theis, A., Seymore, J., Hey, M., Borrmann, S., Diehl, K., Mitra, S. K., and Szakáll, M.: Retention During Freezing of Raindrops, Part I: Investigation of Single and Binary Mixtures, <https://doi.org/10.5194/egusphere-2024-3917>, 19 December 2024.

Goss, K. U.: Adsorption of Organic Vapors on Ice and Quartz Sand at Temperatures Below 0°C , *Environ Sci Technol*, 27, 2826–2830, https://doi.org/10.1021/ES00049A024/ASSET/ES00049A024.FP.PNG_V03, 1993.

- 715 Griessen, R. and Dam, B.: Simple Accurate Verification of Enthalpy-Entropy Compensation and Isoequilibrium Relationship, *ChemPhysChem*, 22, 1774–1784, <https://doi.org/10.1002/CPHC.202100431>, 2021.
- Grosjean, D., Ii, E. L. W., and Grosjean, E.: Atmospheric Chemistry of Isoprene and of Its Carbonyl Products, *Environ. Sci. Technol*, 830–840 pp., 1993.
- Grunwald, E. and Steel, C.: Solvent Reorganization and Thermodynamic Enthalpy-Entropy Compensation, *J. Am. Chem. Soc.*, 5687–5692 pp., 1995.
- 720 Von Hessberg, P., Pouvesle, N., Winkler, A. K., Schuster, G., and Crowley, J. N.: Interaction of formic and acetic acid with ice surfaces between 187 and 227 K. Investigation of single species- and competitive adsorption, *Physical Chemistry Chemical Physics*, 10, 2345–2355, <https://doi.org/10.1039/B800831K>, 2008.
- 725 Heymsfield, A. J., Schmitt, C., Chen, C. C. J., Bansemer, A., Gettelman, A., Field, P. R., and Liu, C.: Contributions of the Liquid and Ice Phases to Global Surface Precipitation: Observations and Global Climate Modeling, *J Atmos Sci*, 77, 2629–2648, <https://doi.org/10.1175/JAS-D-19-0352.1>, 2020.
- Hoareau, C., Noel, V., Chepfer, H., Vidot, J., Chiriaco, M., Bastin, S., Reverdy, M., and Cesana, G.: Remote sensing ice supersaturation inside and near cirrus clouds: a case study in the subtropics, *Atmospheric Science Letters*, 17, 639–645, <https://doi.org/10.1002/ASL.714>, 2016.
- 730 Hudson, P. K., Zondlo, M. A., and Tolbert, M. A.: The interaction of methanol, acetone, and acetaldehyde with ice and nitric acid-doped ice: Implications for cirrus clouds, *Journal of Physical Chemistry A*, 106, 2882–2888, <https://doi.org/10.1021/jp012718m>, 2002.
- Huffman, W. A. and Snider, J. R.: Ice-oxyhydrocarbon interactions in the troposphere, *Journal of Geophysical Research: Atmospheres*, 109, <https://doi.org/10.1029/2003jd003778>, 2004.
- Jacob, D.: INTRODUCTION TO ATMOSPHERIC CHEMISTRY, 11th ed., 2021.
- 735 Jayne, J. T., Duan, S. X., Davidovits, P., Worsnop, D. R., Zahniser, M. S., and Kolb, C. E.: Uptake of gas-phase alcohol and organic acid molecules by water surfaces, *Journal of Physical Chemistry*, 95, 6329–6336, https://doi.org/10.1021/J100169A047/ASSET/J100169A047.FP.PNG_V03, 1991.
- 740 Jost, A., Szakáll, M., Diehl, K., Mitra, S. K., and Borrmann, S.: Chemistry of riming: The retention of organic and inorganic atmospheric trace constituents, *Atmos Chem Phys*, 17, 9717–9732, <https://doi.org/10.5194/ACP-17-9717-2017>, 2017.
- Kahnt, A., Inuma, Y., Böge, O., Mutzel, A., and Herrmann, H.: Denuder sampling techniques for the determination of gas-phase carbonyl compounds: A comparison and characterisation of in situ and ex situ derivatisation methods, *J Chromatogr B Analyt Technol Biomed Life Sci*, 879, 1402–1411, <https://doi.org/10.1016/j.jchromb.2011.02.028>, 2011.
- 745 Krug, R. R., Hunter, W. G., and Grieger, R. A.: Statistical interpretation of enthalpy–entropy compensation, *Nature* 1976 261:5561, 261, 566–567, <https://doi.org/10.1038/261566a0>, 1976.
- Von Kuhlmann, R. and Lawrence, M. G.: The impact of ice uptake of nitric acid on atmospheric chemistry, *Atmos. Chem. Phys*, 225–235 pp., 2006.
- 750 Leffler, J. E.: The enthalpy-entropy relationship and its implications for organic chemistry, *J. org. Chem.*, 20, 1202–1231, <https://doi.org/10.1021/jo01126a009>, 1955.
- Leung, D. H., Bergman, R. G., and Raymond, K. N.: Enthalpy-entropy compensation reveals solvent reorganization as a driving force for supramolecular encapsulation in water, *J Am Chem Soc*, 130, 2798–2805, <https://doi.org/10.1021/ja075975z>, 2008.

- 755 Ling, Z., Xie, Q., Shao, M., Wang, Z., Wang, T., Guo, H., and Wang, X.: Formation and sink of glyoxal and methylglyoxal in a polluted subtropical environment: Observation-based photochemical analysis and impact evaluation, *Atmos Chem Phys*, 20, 11451–11467, <https://doi.org/10.5194/acp-20-11451-2020>, 2020.
- Liu, L. and Guo, Q. X.: Isokinetic relationship, isoequilibrium relationship, and enthalpy-entropy compensation, <https://doi.org/10.1021/cr990416z>, March 2001.
- 760 Liu, Q., Gao, Y., Huang, W., Ling, Z., Wang, Z., and Wang, X.: Carbonyl compounds in the atmosphere: A review of abundance, source and their contributions to O₃ and SOA formation, *Atmos Res*, 274, 106184, <https://doi.org/10.1016/J.ATMOSRES.2022.106184>, 2022.
- Lumry, R.: [29] On the interpretation of data from isothermal processes, in: *Methods in Enzymology*, vol. 259, Academic Press, 628–720, [https://doi.org/10.1016/0076-6879\(95\)59065-X](https://doi.org/10.1016/0076-6879(95)59065-X), 1995.
- 765 Lumry, R. and Rajender, S.: Enthalpy–entropy compensation phenomena in water solutions of proteins and small molecules: A ubiquitous property of water, *Biopolymers*, 9, 1125–1227, <https://doi.org/10.1002/bip.1970.360091002>, 1970.
- Mitra, S. K., Barth, S., and Pruppacher, H. R.: A laboratory study on the scavenging of SO₂ by snow crystals, *Atmospheric Environment. Part A. General Topics*, 24, 2307–2312, [https://doi.org/10.1016/0960-1686\(90\)90324-G](https://doi.org/10.1016/0960-1686(90)90324-G), 1990.
- 770 Moulik, S. P., Naskar, B., and Rakshit, A. K.: Current Status of Enthalpy–Entropy Compensation Phenomenon, *Curr Sci*, 117, 1286, <https://doi.org/10.18520/cs/v117/i8/1286-1291>, 2019.
- Mu, Y. and Xu, Z.: Scavenging of carbonyl sulfide precursor in the atmosphere by precipitation, *Journal of Geophysical Research: Atmospheres*, 114, <https://doi.org/10.1029/2008JD010622>, 2009.
- 775 Mülmenstädt, J., Sourdeval, O., Delanoë, J., and Quaas, J.: Frequency of occurrence of rain from liquid-, mixed-, and ice-phase clouds derived from A-Train satellite retrievals, *Geophys Res Lett*, 42, 6502–6509, <https://doi.org/10.1002/2015GL064604>, 2015.
- Orem, M. W. and Adamson, A. W.: Physical adsorption of vapor on ice: II. n-alkanes, *J Colloid Interface Sci*, 31, 278–286, [https://doi.org/10.1016/0021-9797\(69\)90337-3](https://doi.org/10.1016/0021-9797(69)90337-3), 1969.
- 780 Pan, A., Biswas, T., Rakshit, A. K., and Moulik, S. P.: Enthalpy-Entropy Compensation (EEC) Effect: A Revisit, *Journal of Physical Chemistry B*, 119, 15876–15884, <https://doi.org/10.1021/acs.jpcc.5b09925>, 2015.
- Perrier, S., Houdier, S., Dominé, F., Cabanes, A., Legagneux, L., Sumner, A. L., and Shepson, P. B.: Formaldehyde in Arctic snow. Incorporation into ice particles and evolution in the snowpack, *Atmos Environ*, 36, 2695–2705, [https://doi.org/10.1016/S1352-2310\(02\)00110-3](https://doi.org/10.1016/S1352-2310(02)00110-3), 2002.
- 785 Reif, F.: *Fundamentals of Statistical and Thermal Physics*. International Student Edition, McGraw-Hill, London, New York, 1965.
- Renard, P., Siekmann, F., Salque, G., Smaani, A., Demelas, C., Coulomb, B., Vassalo, L., Ravier, S., Temime-Roussel, B., Voisin, D., and Monod, A.: Aqueous phase oligomerization of methyl vinyl ketone through photooxidation – Part 1: Aging processes of oligomers, <https://doi.org/10.5194/acpd-14-15283-2014>, 12 June 2014.
- 790 Roth, C. M., Goss, K. U., and Schwarzenbach, R. P.: Sorption of diverse organic vapors to snow, *Environ Sci Technol*, 38, 4078–4084, <https://doi.org/10.1021/ES0350684>, 2004.
- Sander, R.: Compilation of Henry’s law constants (version 5.0.0) for water as solvent, *Atmos Chem Phys*, 23, 10901–12440, <https://doi.org/10.5194/ACP-23-10901-2023>, 2023.
- Santachiara, G., Prodi, F., Udisti, R., and Prodi, A.: Scavenging of SO₂ and NH₃ during growth of ice, *Atmos Res*, 47–48, 209–217, [https://doi.org/10.1016/S0169-8095\(97\)00087-2](https://doi.org/10.1016/S0169-8095(97)00087-2), 1998.

- 795 Seymore, J., Gautam, M., Szakáll, M., Theis, A., Hoffmann, T., Ma, J., Zhou, L., and Vogel, A.: Retention During Freezing of Raindrops, Part II: Investigation of Ambient Organics from Beijing Urban Aerosol Samples, <https://doi.org/10.5194/egusphere-2024-3940>, 20 December 2024.
- Sharp, K.: Entropy—enthalpy compensation: Fact or artifact?, *Protein Science*, 10, 661–667, <https://doi.org/10.1110/ps.37801>, 2001.
- 800 Sokolov, O. and Abbatt, J. P. D.: Adsorption to ice of n-alcohols (ethanol to 1-hexanol), acetic acid, and hexanal, *Journal of Physical Chemistry A*, 106, 775–782, <https://doi.org/10.1021/JP013291M/ASSET/IMAGES/MEDIUM/JP013291ME00004.GIF>, 2002.
- Sonntag, D.: Fortschritte in der Hygrometrie, *Meteorologische Zeitschrift*, 3, 51–66, <https://doi.org/10.1127/metz/3/1994/51>, 1994.
- 805 Srivastava, D., Vu, T. V., Tong, S., Shi, Z., and Harrison, R. M.: Formation of secondary organic aerosols from anthropogenic precursors in laboratory studies, *npj Climate and Atmospheric Science* 2022 5:1, 5, 1–30, <https://doi.org/10.1038/s41612-022-00238-6>, 2022.
- Su, S., Xie, Q., Lang, Y., Cao, D., Xu, Y., Chen, J., Chen, S., Hu, W., Qi, Y., Pan, X., Sun, Y., Wang, Z., Liu, C.-Q., Jiang, G., and Fu, P.: High Molecular Diversity of Organic Nitrogen in Urban Snow in North China, *Environ Sci Technol*, <https://doi.org/10.1021/acs.est.0c06851>, 2021.
- 810 Valdez, M. P., Dawson, G. A., and Bales, R. C.: Sulfur dioxide incorporation into ice depositing from the vapor, *J Geophys Res*, 94, 1095–1103, <https://doi.org/10.1029/JD094ID01P01095>;WGROU:STRING:PUBLICATION, 1989.
- 815 Wang, J., Chen, S., Qiu, X., Niu, W., Li, O., Zhu, C., Zhang, X., Yang, X., and Zhang, G.: Pollution Characteristics of Atmospheric Carbonyl Compounds in a Large City of Northern China, *J Chem*, 2022, 3292598, <https://doi.org/10.1155/2022/3292598>, 2022.
- Warhaft, Zellman.: *An Introduction to Thermal-fluid Engineering: The Engine and The Atmosphere*, Cambridge University Press, 266 pp., 1998.
- 820 Winkler, A. K., Holmes, N. S., and Crowley, J. N.: Interaction of methanol, acetone and formaldehyde with ice surfaces between 198 and 223 K, *Physical Chemistry Chemical Physics*, 4, 5270–5275, <https://doi.org/10.1039/b206258e>, 2002.
- Xu, Y., Feng, X., Chen, Y., Zheng, P., Hui, L., Chen, Y., Yu, J. Z., and Wang, Z.: Development of an enhanced method for atmospheric carbonyls and characterizing their roles in photochemistry in subtropical Hong Kong, *Science of The Total Environment*, 896, 165135, <https://doi.org/10.1016/J.SCITOTENV.2023.165135>, 2023.
- 825 Yu, L., Smith, J., Laskin, A., Anastasio, C., Laskin, J., and Zhang, Q.: Chemical characterization of SOA formed from aqueous-phase reactions of phenols with the triplet excited state of carbonyl and hydroxyl radical, *Atmos Chem Phys*, 14, 13801–13816, <https://doi.org/10.5194/ACP-14-13801-2014>, 2014.
- 830 Zhao, M. and Shi, X.: A Study on the Wide Range of Relative Humidity in Cirrus Clouds Using Large-Ensemble Parcel Model Simulations, *Atmosphere* 2023, Vol. 14, Page 583, 14, 583, <https://doi.org/10.3390/ATMOS14030583>, 2023.
- Zhao, Y. H., Abraham, M. H., and Zissimos, A. M.: Fast calculation of van der Waals volume as a sum of atomic and bond contributions and its application to drug compounds, *Journal of Organic Chemistry*, 68, 7368–7373, <https://doi.org/10.1021/jo034808o>, 2003.
- 835 Zondlo, M. A., Barone, S. B., and Tolbert, M. A.: Uptake of HNO₃ on ice under upper tropospheric conditions, *Geophys Res Lett*, 24, 1391–1394, <https://doi.org/10.1029/97GL01287>, 1997.

